

RESEARCH ARTICLE | DECEMBER 28 2021

## Quantum-classical hybrid algorithm for the simulation of all-electron correlation FREE

Jan-Niklas Boyn ; Aleksandr O. Lykhin ; Scott E. Smart ; Laura Gagliardi ; David A. Mazziotti

Check for updates

*J. Chem. Phys.* 155, 244106 (2021)  
<https://doi.org/10.1063/5.0074842>

CHORUS

View  
Online

Export  
Citation

### Articles You May Be Interested In

MC-PDFT can calculate singlet–triplet splittings of organic diradicals

*J. Chem. Phys.* (February 2018)

Extended separated-pair approximation for transition metal potential energy curves

*J. Chem. Phys.* (March 2020)

Efficient algorithm for multiconfiguration pair-density functional theory with application to the heterolytic dissociation energy of ferrocene

*J. Chem. Phys.* (January 2017)

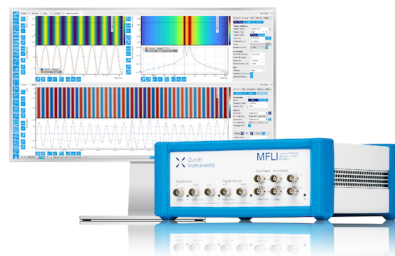
## Challenge us.

What are your needs for periodic signal detection?



Zurich  
Instruments

[Find out more](#)



# Quantum-classical hybrid algorithm for the simulation of all-electron correlation

Cite as: J. Chem. Phys. 155, 244106 (2021); doi: 10.1063/5.0074842

Submitted: 11 October 2021 • Accepted: 2 December 2021 •

Published Online: 28 December 2021



View Online



Export Citation



CrossMark

Jan-Niklas Boyn,<sup>a</sup> Aleksandr O. Lykhin,<sup>a</sup> Scott E. Smart,<sup>a</sup> Laura Gagliardi,<sup>a</sup> and David A. Mazziotti<sup>b</sup>

## AFFILIATIONS

Department of Chemistry and The James Franck Institute, The University of Chicago, Chicago, Illinois 60637, USA

<sup>a</sup>Electronic mail: lgagliardi@uchicago.edu

<sup>b</sup>Author to whom correspondence should be addressed: damazz@uchicago.edu

## ABSTRACT

While chemical systems containing hundreds to thousands of electrons remain beyond the reach of quantum devices, hybrid quantum-classical algorithms present a promising pathway toward a quantum advantage. Hybrid algorithms treat the exponentially scaling part of the calculation—the static correlation—on the quantum computer and the non-exponentially scaling part—the dynamic correlation—on the classical computer. While a variety of algorithms have been proposed, the dependence of many methods on the total wave function limits the development of easy-to-use classical post-processing implementations. Here, we present a novel combination of quantum and classical algorithms, which computes the all-electron energy of a strongly correlated molecular system on the classical computer from the 2-electron reduced density matrix (2-RDM) evaluated on the quantum device. Significantly, we circumvent the wave function in the all-electron calculations by using density matrix methods that only require input of the statically correlated 2-RDM. Although the algorithm is completely general, we test it with two classical density matrix methods, the anti-Hermitian contracted Schrödinger equation (ACSE) and multiconfiguration pair-density functional theories, using the recently developed quantum ACSE method for simulating the statically correlated 2-RDM. We obtain experimental accuracy for the relative energies of all three benzyne isomers and thereby demonstrate the ability of the developed algorithm to achieve chemically relevant and accurate results on noisy intermediate-scale quantum devices.

Published under an exclusive license by AIP Publishing. <https://doi.org/10.1063/5.0074842>

## I. INTRODUCTION

Since the advent of density functional theory (DFT),<sup>1</sup> electronic structure theory has assumed an ever more important role in chemical research from helping researchers rationalize experiment to guiding design in areas ranging from molecular synthesis to new materials. While research over the last decades has made incredible progress in developing accurate and black-box methods available for use by both theoreticians and experimentalists, the accurate as well as computationally tractable treatment of correlated quantum systems continues to pose a major challenge.<sup>2</sup> Quantum simulation of molecular systems offers a novel approach to the problem where a strongly correlated wave function can potentially be prepared and measured at non-exponential cost.<sup>3</sup>

In this article, we present a novel hybrid quantum-classical algorithm that treats the exponentially scaling part of the calculation—the static (multireference) correlation—on the quantum computer and the non-exponentially scaling part—the

dynamic correlation—on the classical computer. While such methods that treat the multireference and dynamic correlation<sup>4,5</sup> in two separate calculations are common in classical electronic structure theory,<sup>2,6–11</sup> their adaptation to the quantum computer is non-trivial because most techniques require a multireference wave function. The measurement of such a wave function on the quantum computer, however, scales exponentially with molecular size.<sup>3,12</sup>

In recent years, a variety of hybrid quantum-classical algorithms have been proposed to overcome this hurdle with the inclusion of dynamic correlation in a “perturb-then-diagonalize” fashion, where the dynamic correlation is resolved before the quantum computations, and thus, no wave function is required for post-processing.<sup>2,13,14</sup> Proposals include integration with DFT<sup>3</sup> or the use of classical embedding algorithms, which tackle only a subset of the problem on the quantum computer in combination with dynamical mean-field theory (DMFT) embedding approaches.<sup>15–17</sup> Additionally, Rubin proposed a density matrix embedding theory (DMET)

analog to the DMFT procedure,<sup>18</sup> and Yamazaki *et al.* proposed further implementations using fragment molecular orbital (FMO) and divide-and-conquer (DC) approaches.<sup>19</sup> Other techniques include the down-folding of active-virtual dynamic correlation using unitary coupled-cluster approaches and a variational quantum eigensolver (VQE),<sup>20–22</sup> or a classically constructed transcorrelated Hamiltonian used in combination with a unitary coupled-cluster ansatz.<sup>23</sup> Post-quantum computation approaches to the inclusion of dynamic correlation have so far proven more challenging, owing to the dependence of many commonplace methods such as multireference perturbation theory on the wave function or higher-order 3- or 4-reduced density matrices (RDMs). One example is the virtual quantum subspace expansion, which perturbs around the singly occupied virtual orbital occupations using an active space 2-RDM.<sup>24,25</sup>

In the approach presented here, as in most molecular simulations, we avoid the exponential scaling by performing a tomography of only the 2-electron reduced density matrix (2-RDM)—more specifically, only the statically correlated part of the 2-RDM.<sup>26</sup> However, in contrast to other methods, we here use the statically correlated 2-RDM as a kernel in two polynomially scaling classical correlation methods to generate a correlated 2-RDM, spanning all of the electrons and orbitals in the calculation, in a “diagonalize-then-perturb” fashion. Importantly, neither method requires computation of the  $N$ -electron wave function and the computed, correlated 2-RDM recovers the all-electron correlation energy of a molecule, thereby enabling larger basis sets and realistic comparisons with experimental enthalpies of formation. Although the algorithm is completely general for any 2-RDM-like methods, we test it here with two classical 2-RDM based methods: (i) the anti-Hermitian contracted Schrödinger equation (ACSE) theory<sup>27</sup> and (ii) multi-configuration pair-density functional theory (MC-PDFT).<sup>28</sup> Additionally, unlike the virtual quantum subspace expansion,<sup>24,25</sup> the present approach in combination with the ACSE is size extensive.

We apply the algorithm to compute the relative energies of the three benzyne isomers to experimental accuracy. The quantum simulation on IBM superconducting quantum computers is performed with the recently developed quantum ACSE (QACSE), an algorithm that belongs to the family of contracted quantum eigensolvers (CQEs) in which a contraction (projection) of the Schrödinger equation is solved for the 2-RDM. While a quantum computer can in theory produce very high-quality results at a lower cost than classical methods, noisy intermediate scale quantum (NISQ) devices exhibit significant noise in their measured quantities such as the 2-RDMs. By using statically correlated 2-RDMs obtained from the QACSE on the IBM quantum computers, we test the ability of the ACSE and MC-PDFT methods to resolve the total energies in the presence of the realistic noise profile of NISQ computers. Importantly, the resulting quantum-classical hybrid algorithm with either ACSE or MC-PDFT for the classical part accurately captures the energies and properties of the benzenes including the experimental relative energy of the biradical *para*-benzyne.

## II. THEORY

Before we present and discuss results in Sec. III, we briefly describe the quantum and classical parts of the hybrid algorithm

in Secs. II A and II B, respectively, which are summarized in Fig. 1.

### A. Contracted quantum eigensolver

The active-space 2-RDMs were obtained using a recently developed contracted quantum eigensolver (CQE) algorithm, known as the quantum-ACSE (QACSE) method<sup>26</sup> (details of these quantum calculations are the focus of a separate work<sup>29</sup>). Unlike the variational quantum eigensolvers, the CQE minimizes the residual of a contraction (projection) of the Schrödinger equation onto a few-electron space. In the QACSE method, we iteratively define an ACSE-ansatz wave function,

$$|\Psi_{n+1}\rangle = e^{\epsilon \hat{A}_n} |\Psi_n\rangle, \quad (1)$$

where

$$\hat{A}_n = \sum_{ijkl}^2 A_{ijkl}^n \hat{a}_i^\dagger \hat{a}_j^\dagger \hat{a}_l \hat{a}_k \quad (2)$$

in which the  ${}^2A^n$  matrices are the residuals of the ACSE

$${}^2A_{ijkl}^n = \langle \Psi_n | [\hat{a}_i^\dagger \hat{a}_j^\dagger \hat{a}_l \hat{a}_k, \hat{H}] | \Psi_n \rangle. \quad (3)$$

These residuals are anti-Hermitian and, hence, can be readily implemented as unitary operators on a quantum computer. By construction, this wave function converges to a solution of the ACSE, which results in the residual vanishing. The two-body nature of the wave function is intrinsically linked to the two-body nature of the ACSE and its residual. The active-space 2-RDM is measured by tomography on the quantum computer without explicit construction of the wave function on the classical computer.

Although the QACSE algorithm is, in principle, exact, in the current era of quantum computing, where only NISQ devices are feasible, several factors must be considered to maximally utilize the present quantum resources. Notably, we truncate elements of  ${}^2A$  to reduce the circuit depth. We also use error mitigation that extends the set of 2-RDMs beyond noise limitations, and then project the 2-RDM onto the 2-positive set of  $N$ -representability conditions to ensure that our 2-RDM is a good representation of a physical system.<sup>30–33</sup> Obtained RDMs from a quantum computer can have substantial errors depending on the noise characteristics of the quantum device, the system size, the quantum algorithm used, and the amount of correlation energy (common errors range from 0.001 to 0.1 hartrees for small systems currently being studied). More details regarding these calculations can be found in the Appendix or Ref. 29.

### B. ACSE and MC-PDFT

To obtain the total electronic energies, we use the classical 2-RDM methods, ACSE and MC-PDFT seeded with the CAS 2-RDM evaluated on the quantum device. On the classical computer, the ACSE can be solved by evolving a system of differential equations.<sup>34,35</sup> Because the ACSE depends on not only the 2-RDM but also the 3-RDM, the ACSE is indeterminate without a reconstruction of the 3-RDM from the 2-RDM. While in the quantum algorithm, this reconstruction occurs implicitly and potentially

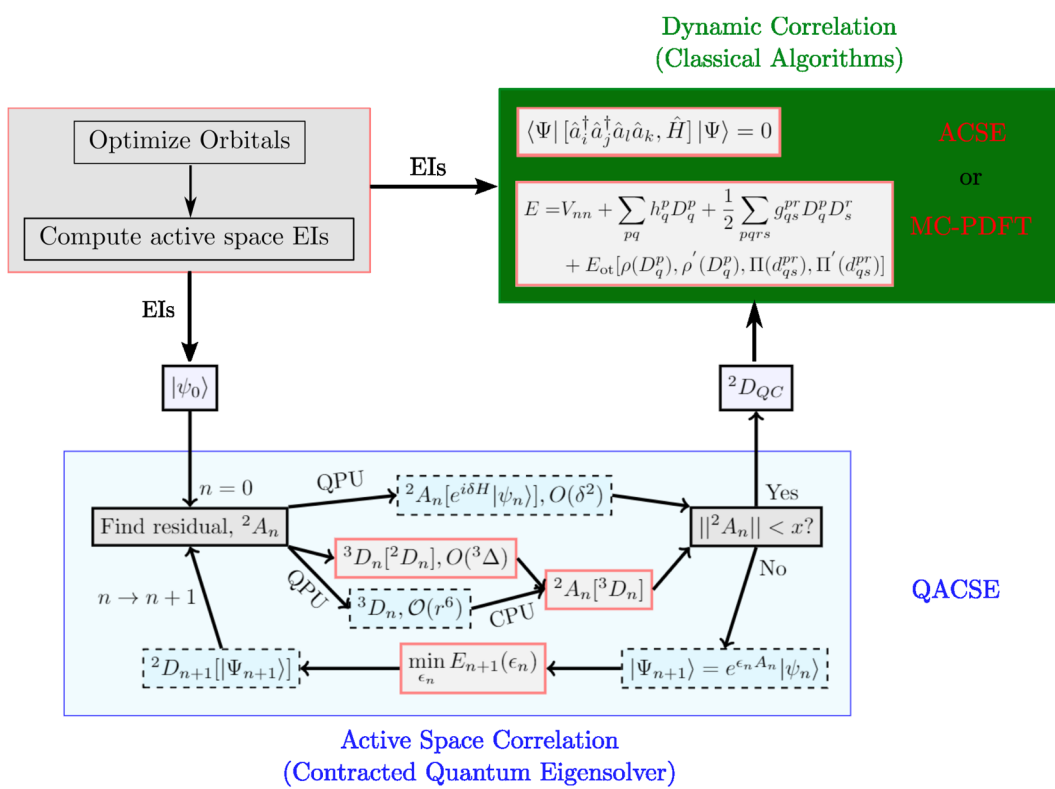


**FIG. 1.** Schematic description of the hybrid quantum-classical algorithm employed in this work. The red boxes denote the calculations performed on a classical computer, while those in blue boxes represent the quantum computations. The QACSE algorithm itself can be considered a hybrid algorithm that possesses corresponding advantages and disadvantages depending on the particular elements that are utilized. For instance, the residual  ${}^2A_n$  classically requires the 3-RDM, which can be obtained from a 2-RDM with an approximate cumulant  ${}^3\Delta$ , or on the quantum computer with  $\mathcal{O}(r^6)$  scaling tomography of the 3-RDM. While an  $\mathcal{O}(r^4)$  method can be performed solely on the quantum computer with a truncated error in  $\delta$ , it requires a longer gate sequence that may not be preferable on near-term devices. Given an operator  ${}^2A$ , we can measure  ${}^2D_{n+1}$  through the preparation of the wave function  $|\psi_{n+1}\rangle$ , and this process is repeated iteratively until the final 2-RDM  ${}^2D_{QC}$  is obtained, which is used to seed the classical ACSE or MC-PDFT algorithms.

exactly through the state preparation on the quantum device, in the classical algorithm, the 3-RDM is approximately reconstructed from the 2-RDM by its cumulant expansion.<sup>36–38</sup> The classical implementation of the ACSE resolves dynamic correlation with comparable accuracy to CCSD(T),<sup>37</sup> but it may be seeded with a correlated guess 2-RDM from a complete active space (CAS) calculation to resolve the total correlation energy even in the presence of non-negligible static electron correlation.<sup>34,35</sup>

MC-PDFT in turn is an extension of DFT to strongly correlated systems. Seeded with a strongly correlated 2-RDM obtained from a CAS calculation, kinetic and classical Coulomb energies are evaluated and the rest of the energy is non-iteratively computed as a function of the total electron density, the on-top pair density, and their spatial derivatives using one of the various available functionals. In this article, we survey translated<sup>28</sup> (tPBE and tBLYP), (ii) fully translated<sup>39</sup> (ftPBE), and (iii) hybrid<sup>40</sup> (tPBE0) on-top functionals. The ACSE calculations were performed with the Maple Quantum Chemistry Package,<sup>41,42</sup> and MC-PDFT calculations were performed in the PySCF package<sup>43</sup> augmented with the *mrh* addon<sup>44</sup> that enables MC-PDFT features.

### III. RESULTS AND DISCUSSION

As a benchmarking case of correlated organic molecules, we consider the three structural isomers of benzene.<sup>45–47</sup> These are obtained by the elimination of two substituents on different positions of the benzene ring, giving rise to *ortho*-, *meta*-, and *para*-isomers. While all benzene isomers are usually drawn as biradical structures, the degree to which they display multi-reference character varies according to the spatial separation between the radical electrons' location on the benzene ring. Figure 2 displays the frontier molecular orbitals for each of the three structural benzene isomers, showing the clear variation in bonding between the *ortho*, *meta*, and *para* geometries. Spatial proximity between the two radical carbon atoms on the benzene ring allows substantial bond formation in the *ortho* and *meta* cases, leading to near-closed-shell character. In contrast the *para* geometry is characterized by a large spatial separation between the radical carbons, which prevents the overlap of the carbon atomic orbitals, resulting in strong biradical character. The stability of the three isomers correlates with the proximity of the radical carbon atoms, with experimental measurements yielding

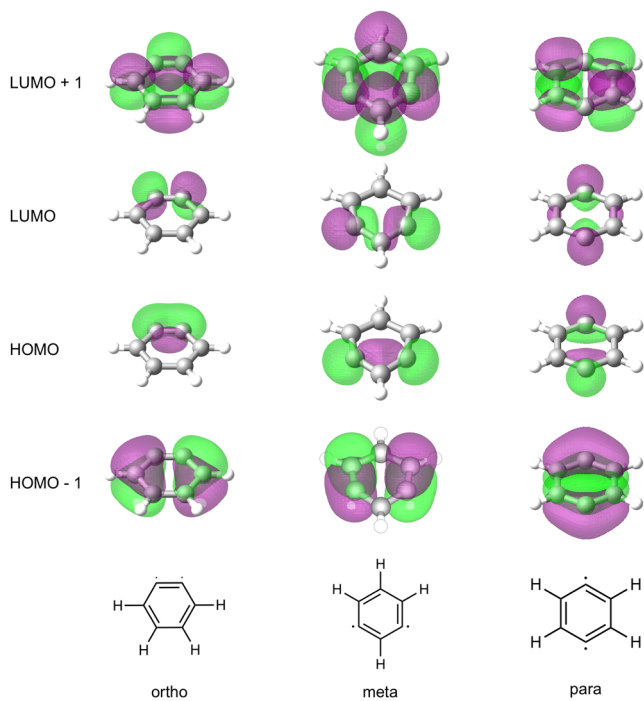


**FIG. 2.** HOMO and LUMO for the three structural benzene isomers as obtained from classical CASSCF calculations in a [4, 4] active space with a cc-pVDZ basis set. The biradical character displayed in the frontier MOs increases as the orbital separation between the radical carbon atoms increases. While spatial proximity allows for the formation of bonding and anti-bonding orbitals in *ortho*- and *meta*-benzyne, yielding near-closed-shell character, the larger distance in the *para*-isomer yields an electronic structure with strong biradical character.

energies of  $15.3 \pm 4.31$  and  $31.2 \pm 4.17$  kcal/mol, for the *meta* and *para* isomers, relative to the *ortho* structure, respectively.<sup>47</sup>

### A. Relative energies

While the complete active space self-consistent field (CASSCF) and configuration interaction (CASCI) methods capture most of the static correlation, they lack a fraction of dynamic correlation resulting in residual errors in the energies of the *ortho*-, *meta*-, and *para*-isomers. Taking the *ortho* isomer as a reference, classical CASSCF calculations with the correlation-consistent polarized double-zeta (cc-pVDZ) basis<sup>48</sup> yield relative energies of 15.2 kcal/mol (*meta*) and 23.5 kcal/mol (*para*) in a [2, 2] active space, which increase to 16.5 kcal/mol (*meta*) and 29.5 kcal/mol (*para*) upon moving to a [4, 4] active space. We use the  $[N_e, N_o]$  active space notation, where  $N_e$  is the number of active electrons and  $N_o$  denotes the number of spatial orbitals in the active space. The active space MOs are those shown in Fig. 2, and both MC-PDFT and ACSE calculations do not profit from the use of larger CASSCF active space seeds as the strong correlation in the benzyne systems is contained in two molecular orbitals. Data for larger [6, 6] and [8, 8] classically seeded calculations are shown in the [supplementary material](#). Using one- and two-electron integrals in the molecular orbital basis from the classical CASSCF calculations, the QACSE has been shown to resolve the relative energies (despite errors in the absolute energies

on the order of a few kcal/mol) of the benzyne isomers with comparable accuracy to classical CASSCF calculations, yielding gaps of 13.8 kcal/mol (*meta*) and 21.7 kcal/mol (*para*) in the [2, 2] active space performed on a 1-qubit device and 17.9 kcal/mol (*meta*), 31.0 kcal/mol (*para*) and 17.6 kcal/mol (*meta*), 27.8 kcal/mol (*para*) in a [4, 4] active space using 3- and 4-qubit calculations, respectively. These results are thoroughly discussed in Ref. 29, and the data are shown in Table S1. Having demonstrated the ability to perform sufficiently accurate CAS calculations on a NISQ device and yielding accurate 2-RDMs with the QACSE method, we take the next step in bringing quantum computing to the realm of applicable quantum-chemical computation by uniting the QACSE with the 2-RDM dependent MC-PDFT and ACSE methods to recover all-electron correlation in a hybrid quantum-classical approach.

The 2-RDMs obtained from the QACSE calculations are used to seed the classical ACSE and various MC-PDFT functionals to calculate the total electronic energy of the three different isomers. The *meta*-*ortho* and *para*-*ortho* energy gaps, obtained with the ACSE and MC-PDFT (tPBE functional) from CASSCF [2, 2] and [4, 4] calculations on a classical computer (CASSCF), as well as a quantum computer (QACSE CASSCF) with 1 qubit, 3 qubits, or 4 qubits, are displayed in Figs. 3(a) and 3(b), while Figs. 3(c) and 3(d) show the respective errors in relative energies as compared to experiment. Using the minimal [2, 2] active space required to resolve the biradical character, both the ACSE and MC-PDFT seeded with the QACSE 2-RDMs deliver results that yield a lower bound to the gap obtained using the classical CASSCF 2-RDM. Deviations from the classically seeded references are less than 2 kcal/mol in the case of the ACSE and less than 7 kcal/mol for tPBE, yielding errors slightly outside the bounds of the experimental confidence intervals.

A move to the larger [4, 4] active space reduces the error of the relative energies in both the underlying classical CASSCF reference and QACSE calculations. Utilizing different symmetry adaptations (see the [Appendix](#)) on the quantum device, the [4, 4] QACSE calculations were carried out using either 3 qubits or 4 qubits, with the 4 qubits producing noisier results. In the post-CASSCF ACSE calculation, favorable error cancellation leads to increases in the *meta*-*ortho* and *para*-*ortho* gaps and correspondingly reduced errors as compared to experiment. The *meta*-*ortho* gap is reproduced within the experimental confidence intervals, yielding gaps of 12.0 and 14.3 kcal/mol for 3- and 4-qubit 2-RDMs, respectively, while the *para*-*ortho* gap of 26.8 kcal/mol in the 3-qubit case lies barely 0.2 kcal/mol outside the experimental interval and is improved to 28.8 kcal/mol with the use of a 4-qubit 2-RDM. It is noteworthy that the *meta*-*ortho* gap is captured with significantly greater accuracy by the ACSE than the *para*-*ortho* gap.

The trend observed in the ACSE data is reversed in the tPBE calculations and in the classically seeded tPBE calculations the magnitude of relative energies is reduced upon moving from a [2, 2] to a [4, 4] active space with the calculated *meta*-*ortho* gap lying slightly outside the experimental confidence interval. However, using the 3-qubit QACSE 2-RDM, we again observe an increase in the calculated relative energies, 11.1 kcal/mol (*meta*-*ortho*) and 33.1 kcal/mol (*para*-*ortho*), which lie within the experimental bounds of error. Using the 2-RDM obtained from 4-qubit NISQ

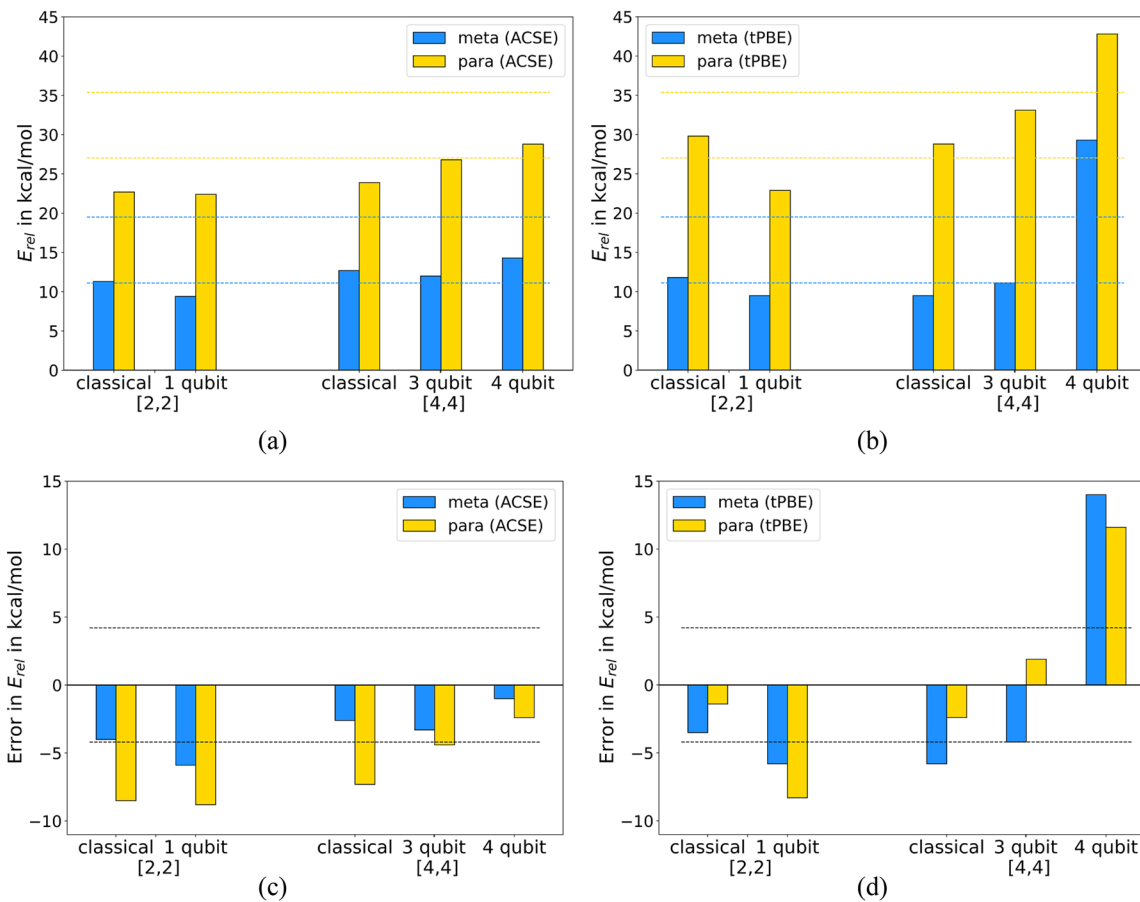


**FIG. 3.** Top row: Relative energies of the *meta* and *para* benzyne calculated with ACSE (a) and MC-PDFT (b). Bottom row: Deviations of the relative energies from the corresponding experimental relative energies of the *meta* and *para* benzyne calculated with ACSE (c) and MC-PDFT (d). The *ortho* isomer serves as the reference to determine energies of *meta* and *para* benzyne. On the x-axis, “classical” refers to the solutions obtained with a CASSCF 2-RDM evaluated on a classical computer, and “1 qubit,” “3 qubit,” and “4 qubit” labels indicate ACSE or MC-PDFT (tPBE functional) calculations seeded with a QACSE 2-RDM measured with 1 qubit, 3 qubits, or 4 qubits, respectively. The active space  $[N_e, N_o]$  refers to  $N_e$  active electrons distributed in  $N_o$  active molecular orbitals. The dashed lines represent uncertainties of the experimental relative energies at the 95% confidence level.

26 October 2024 18:04:31

device calculation, the MC-PDFT energies are more prone to errors propagated from noisy 2-RDMs, resulting in significant overestimation of *meta-ortho* and *para-ortho* gaps. The sign change in the errors of the relative energies in MC-PDFT as we move from 3 qubits to 4 qubits occurs because the noise of the 4-qubit QACSE 2-RDM leads to an energy of the *ortho* isomer that is too low, which overstabilizes that isomer relative to the *meta* and *para* isomers. Absolute energies are discussed in more detail in Sec. III B.

In addition to tPBE, we also survey the ftPBE, trevPBE, tBLYP, and tPBE0 functionals. The complete data for the *meta-ortho* and *para-ortho* energy gaps for all methods are shown in Table S1. The choice of the on-top functional does not significantly affect the predicted relative energies of the three benzyne diradicals in MC-PDFT. The energies obtained with the fully translated functional ftPBE yield the most accurate results; however, they present only slight improvements upon the tPBE, trevPBE, and tBLYP

results. The hybrid tPBE0 on-top functional is an outlier in the set of surveyed functionals and it results in large deviations from the experimental energies, particularly in the *para-ortho* 4-qubit calculations.

Our data show that efficient error mitigation in the QACSE algorithm allows us to obtain strongly correlated 2-RDMs on a NISQ device sufficiently purified so that they may be used to seed ACSE and MC-PDFT calculations to compute all-electron correlation with near-classical accuracy. While noise increases with the number of qubits used in the quantum computation, in the case of benzyne, both the ACSE and MC-PDFT seeded with the NISQ derived 2-RDM allow us to resolve an experimentally verifiable quantity, the relative energies of the three structural isomers, with an accuracy that lies within the bounds of the experimental confidence intervals for a [4, 4] CAS calculation implemented with a 3-qubit mapping.

## B. Absolute energies

To further analyze the impact of NISQ-derived QACSE 2-RDMs on ACSE and MC-PDFT calculations in a quantum-classical hybrid implementation, we compare the obtained absolute energies to those yielded with a CASSCF seed. Figure 4 shows the mean absolute errors, defined as  $\text{MAE} = \sum_{m,o,p} |E_q - E_c|/3$ , where  $\sum_{m,o,p}$  runs over the three isomers,  $E_q$  indicates the quantum calculation's energy, and  $E_c$  indicates the energy derived from the classical reference calculation, for the QACSE, the QACSE/ACSE, and QACSE/tPBE calculations of the total electronic energy for the three benzyne isomers. The QACSE calculation yields energies that in these cases are above those from the classical CASSCF calculation, and as expected, the magnitude of the deviation increases with increasing qubit count and correspondingly greater noise in the quantum device measurements. The deviations for the absolute energies of the individual isomers can be found in Table I.

The same behavior is observed in the QACSE/ACSE calculations, which when seeded with a quantum computed 2-RDM yield energies above those from the QACSE/ACSE calculations seeded with classical CASSCF for all but the 3-qubit *meta*-benzyne case. In the [2, 2] case, the error from the QACSE with an MAE of 1.96 kcal/mol persists in the ACSE solution with its MAE of 2.29 kcal/mol. In contrast, errors are reduced in the [4, 4] calculations. Here, while the error obtained by the QACSE/ACSE calculation for the *para* isomer remains nearly identical to that of the underlying CAS calculation, we obtain significantly reduced errors in the *ortho* and *meta* isomers. The MAE of 1.22 kcal/mol presents a notable reduction compared to the underlying QACSE that displayed a MAE of 3.41 kcal/mol. While the noisier 4-qubit calculation produces larger deviations from the classical results, the errors in the QACSE again do not completely propagate to the post-CI ACSE calculation, and instead the errors in the underlying QACSE calculation

**TABLE I.** Deviations in kcal/mol from the classical, or classically seeded calculation,  $\Delta E = E_{qc} - E_c$ , where  $E_{qc}$  denotes the QACSE CASSCF energy, or the ACSE or tPBE energy when seeded with the QACSE 2-RDM, and  $E_c$  denotes the classical CASSCF energy, or the ACSE or tPBE energy obtained with a CASSCF 2-RDM.

			Error in kcal/mol		
			QACSE	ACSE	tPBE
[2, 2]	1 qubit	<i>ortho</i>	3.03	4.39	8.99
		<i>meta</i>	1.64	2.46	6.71
		<i>para</i>	1.21	4.04	2.18
[4, 4]	3 qubit	<i>ortho</i>	1.31	0.08	-3.30
		<i>meta</i>	2.72	-0.62	-1.65
		<i>para</i>	2.83	2.96	1.08
		<i>ortho</i>	12.36	6.63	-7.52
[4, 4]	4 qubit	<i>meta</i>	13.45	8.25	12.32
		<i>para</i>	10.67	11.59	6.57

are reduced significantly by  $\Delta\text{MAE} = 3.33$  kcal/mol in the post-CI result.

Similar trends are observed using MC-PDFT functionals. Here, tPBE yields increased errors over the CAS calculation alone when seeded with the [2, 2] QACSE 2-RDM, while reduced errors compared to the CAS calculation alone are obtained in the two studied [4, 4] settings, with reductions in MAE of 0.3 kcal/mol and 3.36 kcal/mol in the 3- and 4-qubit cases, respectively. Note that in MC-PDFT errors are lowest in the *meta* and *para* isomers, while the use of the QACSE solution leads to a large negative deviation from the CASSCF/MC-PDFT solution in the *ortho* case, where a lower bound to the classical solution is obtained. This is observed in both the 3-qubit and 4-qubit [4, 4] calculations, but not in the [2, 2] 1-qubit case.

Additional insight into the nature of errors introduced via the use of NISQ-device-derived 2-RDMs in the ACSE and MC-PDFT calculations may be obtained by decomposing the total electronic energy into its individual 1- and 2-electron components. This analysis can be found in Sec. II of the [supplementary material](#).

## C. Orbital occupation numbers

Finally, we consider the impact of the use of a quantum computed 2-RDM on the natural occupation numbers (NONs) obtained from the classical dynamical correlation calculations. As MC-PDFT does not reoptimize the 2-RDM and orbital occupations, we only consider the ACSE results. Table II shows the NONs for the CAS and ACSE calculations for both classical and quantum computations. Generally, a more correlated solution is characterized by more fractional NONs. According to deviations of the NONs from 0 and 1 with greater deviations indicating more correlation, the quantum CAS (QACSE) results are more correlated than the classical CASSCF results for all three isomers in the [2, 2] active space and for the more strongly correlated *meta* and *para* isomers in the [4, 4] active space. The use of 4 qubits over 3 qubits yields reduced correlation in the *ortho* isomer and increased correlation in the *meta* and *para* isomers. While the dynamic correlation introduced by the post-CI ACSE calculation yields a more correlated solution via the

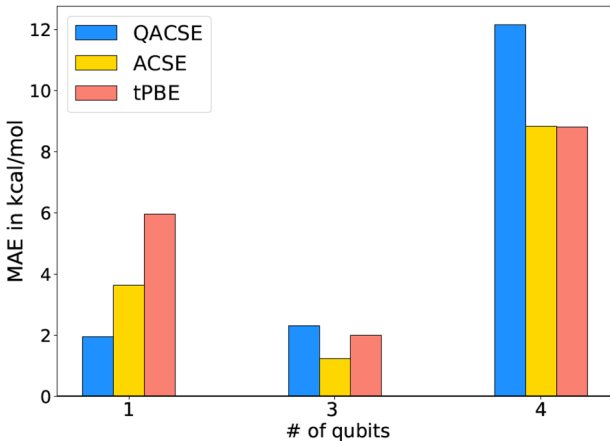


**FIG. 4.** MAEs in kcal/mol of the quantum solution with respect to the classical reference over the three isomers for the QACSE CAS, as well as the QACSE 2-RDM seeded ACSE and tPBE functional MC-PDFT calculations. 1-qubit data use a [2, 2] active space, while the 3- and 4-qubit data were obtained with a [4, 4] active space.

**TABLE II.** Natural occupation numbers (NONs) of the HONO and LUNO for the CASSCF and QACSE calculations (CAS column) and as well as the QACSE and CASSCF seeded ACSE calculations (ACSE column).

		CAS		ACSE	
		HONO	LUNO	HONO	LUNO
[2, 2]	<i>ortho</i>	Classical	0.905	0.095	0.886
		1 qubit	0.845	0.155	0.833
	<i>meta</i>	Classical	0.855	0.145	0.837
		1 qubit	0.800	0.200	0.787
	<i>para</i>	Classical	0.615	0.385	0.608
		1 qubit	0.565	0.435	0.558
[4, 4]	<i>ortho</i>	Classical	0.905	0.095	0.888
		3 qubit	0.925	0.075	0.904
		4 qubit	0.970	0.025	0.943
	<i>meta</i>	Classical	0.880	0.120	0.859
		3 qubit	0.880	0.120	0.861
		4 qubit	0.785	0.215	0.771
	<i>para</i>	Classical	0.615	0.385	0.610
		3 qubit	0.575	0.425	0.568
		4 qubit	0.600	0.395	0.593

inclusion of core and virtual orbital contributions, the changes in HONO and LUNO occupations that are relevant for the capture of the biradical character displayed by the benzenes are minor compared to the magnitude of the multi-reference character obtained by the QACSE and CASSCF calculations. Consequently, we see a strong dependence on the initial results of the QACSE calculation in the QACSE/ACSE results and as such, computations involving the NISQ device to obtain active space 2-RDMs tend to yield more multi-reference character and more partial HONO and LUNO NON in a post-processing ACSE calculation when compared to the classical reference.

#### IV. CONCLUSIONS

Realizing the unique position of the ACSE and MC-PDFT as possible post-processing methods to compute all-electron correlation in hybrid quantum-classical algorithms owing to their dependence on only the 2-RDM rather than the  $N$ -electron wave function, we have successfully used them in tandem with NISQ-CAS calculations, performed with the QACSE contracted quantum eigensolver, to resolve the total electronic correlation energy of the isomers of benzene. We have demonstrated that 2-RDMs from NISQ devices, after error mitigation with necessary  $N$ -representability conditions, allow for the resolution of an experimentally verifiable quantity, the relative energies of the different benzene isomers, within the bounds of the experimental margins of error in a QACSE/ACSE and QACSE/MC-PDFT hybrid classical-quantum algorithm. Furthermore, we have shown that the errors arising in CAS calculations on NISQ devices are not necessarily amplified in post-correction ACSE and MC-PDFT calculations relying on their 2-RDMs. Instead, in the noisier 3- and 4-qubit calculations, we observe a reduction in the error compared to the respective classical analogs when comparing the absolute energies of the CAS and post-CI

calculations. Thus, classical post-correction calculations of the total correlation energy, as implemented in QACSE/ACSE and QACSE/MC-PDFT, may play an additional role as further sources of error mitigation in the applications of quantum algorithms.

While we have focused on ACSE and MC-PDFT, other 2-RDM-based methods—methods that require only an input 2-RDM rather than the many-electron wave function or higher RDMs—can also be employed within the general hybrid quantum-classical algorithmic framework proposed here. For example, a recent extension of the quantum subspace expansion (which itself is closely related to the classical methods for extracting excited states from the 2-RDM<sup>49–51</sup>), called the virtual quantum subspace expansion,<sup>24,25</sup> adds correlation to an initial 2-RDM through single and double excitations. Unlike the ACSE, however, this method is not necessarily size-extensive.

With the advances reported in this article, we successfully take a first step in bringing NISQ device-based hybrid quantum-classical algorithms into the realm of everyday computational chemistry applications. Even as quantum hardware markedly improves, the quantum-classical quantum algorithm presented here, including the 2-RDM-based error mitigation, will be critically important for merging the strengths of quantum and classical computers for accurately simulating the energies and properties of chemically important molecules and materials.<sup>2,3,8,13,52</sup>

#### SUPPLEMENTARY MATERIAL

The [supplementary material](#) contains additional data on active-space convergence, relative energies, energy decompositions, quantum simulation errors, and computational scripts.

#### ACKNOWLEDGMENTS

D.A.M. acknowledges funding from the U.S. Department of Energy (Office of Basic Energy Sciences) under Award No. DE-SC0019215 and the U.S. National Science Foundation under Award Nos. CHE-2035876 and CHE-1565638. A.O.L. and L.G. acknowledge funding from the Division of Chemical Sciences, Geosciences, and Biosciences, Office of Basic Energy Sciences of the U.S. Department of Energy, through Grant No. DE-SC002183. We acknowledge the use of IBM Quantum services for this work. The views expressed are those of the authors and do not reflect the official policy or position of IBM or the IBM Quantum team.

#### AUTHOR DECLARATIONS

##### Conflict of Interest

The authors have no conflicts to disclose.

#### DATA AVAILABILITY

The data that support the findings of this study are available within the article and its [supplementary material](#).

#### APPENDIX: METHODS

##### 1. ACSE

The  $N$ -electron Schrödinger equation may be contracted onto the space of pairwise excitations, giving rise to the contracted

Schrödinger equation (CSE),<sup>53</sup>

$$\langle \Psi | \hat{a}_i^\dagger \hat{a}_j^\dagger \hat{a}_l \hat{a}_k \hat{H} | \Psi \rangle = E^2 D_{kl}^{ij}, \quad (\text{A1})$$

where  $\hat{a}^\dagger$  and  $\hat{a}$  are the fermionic creation and annihilation operators, respectively, and  $\hat{H}$  is the electronic Hamiltonian,

$$\hat{H} = \sum_{ij} K_j^i \hat{a}_i^\dagger \hat{a}_j + \sum_{ijkl} V_{kl}^{ij} \hat{a}_i^\dagger \hat{a}_j^\dagger \hat{a}_l \hat{a}_k. \quad (\text{A2})$$

The CSE may be expanded into its Hermitian and anti-Hermitian parts,

$$\left\langle \Psi \left| \left\{ \hat{a}_i^\dagger \hat{a}_j^\dagger \hat{a}_l \hat{a}_k, (\hat{H} - E) \right\} \right| \Psi \right\rangle + \left\langle \Psi \left| \left[ \hat{a}_i^\dagger \hat{a}_j^\dagger \hat{a}_l \hat{a}_k, (\hat{H} - E) \right] \right| \Psi \right\rangle = 0, \quad (\text{A3})$$

where the square and curly brackets denote the commutator and anti-commutator, respectively. While the CSE depends on the 2-, 3-, and 4-reduced density matrix (RDM), we can select just the anti-Hermitian part of the CSE, yielding the anti-Hermitian contracted Schrödinger equation (ACSE), which in turn only depends on the 2- and 3-RDMs,<sup>27,34,35,53–55</sup>

$$\left\langle \Psi \left| \left[ \hat{a}_i^\dagger \hat{a}_j^\dagger \hat{a}_l \hat{a}_k, \hat{H} \right] \right| \Psi \right\rangle = 0. \quad (\text{A4})$$

The computationally expensive dependence on the 3-RDM may be further simplified by employing cumulant reconstruction, allowing the 3-RDM elements to be approximately reconstructed in terms of the 2-RDM elements,<sup>38,53,56</sup>

$${}^3D_{qst}^{ijk} \approx {}^1D_q^i \wedge {}^1D_s^j \wedge {}^1D_t^k + 3 \Delta_{qs}^{ij} \wedge {}^1D_t^k, \quad (\text{A5})$$

where

$$2 \Delta_{qs}^{ij} = {}^2D_{qs}^{ij} - {}^1D_q^i \wedge {}^1D_s^j \quad (\text{A6})$$

and  $\wedge$  denotes the antisymmetric Grassmann wedge product,<sup>53</sup> which is defined as

$${}^1D_k^i \wedge {}^1D_l^j = \frac{1}{2} \left( {}^1D_k^i {}^1D_l^j - {}^1D_l^j {}^1D_k^i \right). \quad (\text{A7})$$

In this implementation, we use the Valdemoro reconstruction, further simplifying our 3-RDM reconstruction by approximating  $\Delta_{qst}^{ijk}$  to be zero.<sup>36,57</sup>

The ACSE is solved via a series of differential equations, where at each step we use the solution of the ACSE to generate an anti-Hermitian operator,  $\hat{A}$ , which is related to the gradient information with respect to various two-body body unitary transformations. Indeed, the exponential of the operator gives a unitary transformation that allows us to minimize the energy against these transformations.<sup>34</sup> If the starting 2-RDM corresponds to the single-reference state, e.g., obtained from a Hartree-Fock calculation, the obtained solutions resolve dynamic correlation effects with accuracy comparable to CCSD(T).<sup>37,58</sup> However, by starting with a multi-reference 2-RDM, which can be obtained from active space methods, the total electron correlation is obtained—not just the static correlation present in a multiconfigurational seed 2-RDM.<sup>34,35,59</sup> This approach has been demonstrated to resolve successfully the chemical and electronic properties in a variety of correlated systems, such as the S-T gaps in small biradicals,<sup>35</sup> the barriers and conical intersections in chemical reactions,<sup>60–62</sup> and excited states<sup>63,64</sup> with accuracy exceeding go-to methods such as multireference configuration

interaction plus a quadratic correction (MRCI+Q) or multireference second-order perturbation theory (MRPT2), and comparable to state-of-the-art methods such as auxiliary-field quantum Monte Carlo (AFQMC).

## 2. QACSE

The quantum ACSE (QACSE) method<sup>26,29</sup> relies upon the capacity of a quantum computer to simulate quantum states efficiently in potentially two regards. First, the exponential of the  $\hat{A}$  operator can be implemented through methods of quantum computation for implementing exponential operators at polynomial cost (see below and Refs. 26 and 29). Then, by performing reduced state tomography, we can measure the 2-RDM of a prepared quantum state at any given iteration. Second, we can use an auxiliary state involving the  $\exp(i\delta H)$  operator to find a solution to the ACSE. If this step cannot be carried out accurately on the quantum computer (through noise or limited quantum resources), then we can use the classical solution of the ACSE, which involves a reconstructed 3-RDM. The tomography naively requires  $\mathcal{O}(r^4)$  measurements, although this can be reduced to  $\mathcal{O}(r^2)$  through a variety of techniques.<sup>65,66</sup>

Third, elements of the  ${}^2A$  matrix can be obtained efficiently through the preparation of an auxiliary state involving a single propagator step. Tomography of the  ${}^2A$  matrix scales with the order of the  $\hat{A}$  operator, which generally will be  $\mathcal{O}(r^4)$ . In both cases, the use of a quantum computer allows us to extract information directly from the quantum state, circumventing the cost and errors that come from reconstruction.<sup>26,29</sup> The algorithm iterates between the preparation of the 2-RDM and the  $A$  matrix until convergence, which is shown in Fig. 1.

## 3. Quantum computation

The 2-RDMs used in the present work were obtained by using quantum devices (ibmq\_armonk for the 1-qubit results, and ibmq\_bogota and ibmq\_santiago, which are 5-qubit devices, for the 3- and 4-qubit results) through the IBM Quantum Experience.<sup>67</sup> We use the PYTHON 3 package QISKit (v 0.15.0–v 0.17.0)<sup>68</sup> to interface with the device. The calculations themselves are multifaceted, with significant error mitigation also being required, and we include a brief overview below.

First, we transform the Hamiltonian to the Pauli basis through the Jordan-Wigner transformation, and then we analyze the set of Hamiltonian operators for Pauli-type symmetries. These can be related to known quantum chemical (i.e., spin, point-group, etc.) symmetries,<sup>69</sup> but in our cases, these should be interpreted simply as symmetries of the transformed Pauli basis. Having  $s$  symmetries, we can obtain a  $2r - s$  qubit representation. For the [4, 4] case, we have 8 spin orbitals, mapping to 8 qubits. The 4-qubit case represents 4 symmetries that are tapered from the Hamiltonian. The *para*-isomer has an exact 3-qubit representation (5 symmetries), whereas *meta*- and *ortho*- have errors in the symmetry representations of 0.61 and 0.92 mhartrees, respectively. Note that these errors are significantly less than the external noise related errors on the relevant quantum devices.

Using the residual  ${}^2A$  matrix generated from the classical ACSE, we map these elements onto the operator basis and create our test ansatz. We use a first-order trotterization to express the  $\exp({}^2A)$  operator, which becomes a product of exponential Pauli strings

(tensors of Pauli gates). The exponential of an anti-Hermitian Pauli operator can be expressed as a sequence of rotated controlled Z gates where the controlled qubits act on a single qubit. Because the pool of operators is quite limited, we simplified likely potential two-body operators for these bases and allowed the ACSE algorithm to choose operators appropriately. Once the gate sequence was prepared, we measured the 2-RDM. We utilized a state preparation technique to counteract readout errors, and then we filtered the diagonal entries so that the trace of the 2-RDM is normalized to the number of electrons. To counter the accumulating effects of noise, which occur with an iterative ansatz, we used a limit-preserving correction, which adds a correction matrix to the 2-RDM so that a new step with zero input parameters will give the same energy as the previous step. This attempts to mitigate the increase in energy caused by adding more gates to an ansatz that commonly occurs. Finally, as some of the previous steps can introduce  $N$ -representability violations, we used a purification scheme so that the obtained 2-RDM satisfies a set of approximate  $N$ -representability conditions. We iterated this procedure until convergence was met, or we were unable to decrease the energy of the state. More details regarding these calculations and error mitigation schemes are found in Ref. 29. For all of these calculations, the error in using an approximate  $^2A$  can vary depending on the ansatz and the optimization of the step size used. We discuss further errors in the QACSE results related to the use of noisy quantum devices in the [supplementary material](#). We include scripts in the [supplementary material](#) showing an example run with the open-source HQCA<sup>70</sup> module. More general scripts can be found in the module itself.

#### 4. MC-PDFT

The multiconfiguration pair-density functional theory (MC-PDFT) is an extension of the density functional theory to the molecular systems with strong electron correlation. The advantage of MC-PDFT is that the correlation energy is computed with a low computational cost compared to the alternative multireference methods, such as multireference second-order perturbation theory (MRPT2)<sup>6</sup> or the multireference configuration interaction (MRCI)<sup>71</sup> method. In MC-PDFT, kinetic and classical Coulomb energies are evaluated from the multiconfigurational wave function represented by 1,2-RDMs, while the rest of the energy is computed non-iteratively as a function of the total electron density, the on-top pair density, and their spatial derivatives,<sup>28</sup>

$$E_{\text{MC-PDFT}} = V_{nn} + \sum_{pq} h_q^p D_q^p + \frac{1}{2} \sum_{pqrs} g_{qs}^{pr} D_q^p D_s^r + E_{\text{tot}}[\rho(D_q^p), \rho'(D_q^p), \Pi(d_{qs}^{pr}), \Pi'(d_{qs}^{pr})]. \quad (\text{A8})$$

While the total electron density,  $\rho$ , defines the probability of locating a single electron at the given point of space, the on-top pair density,  $\Pi$ , describes the probability of observing two electrons at the same space point. The dependence of the functional upon these densities, conveniently evaluated from 1,2-RDMs, resolves the symmetry dilemma<sup>72</sup> and ensures the correct asymptotic behavior of the total energy at the dissociation limit. In general, any type of multiconfigurational reference can be exploited in MC-PDFT. The most common choices are state-specific and state-averaged complete active space self-consistent field (SS-CASSCF

and SA-CASSCF) wave functions;<sup>73–76</sup> however, other multiconfigurational wave functions have also been successfully combined with MC-PDFT including those obtained with restricted active space self-consistent field (RASSCF)<sup>77,78</sup> restricted active space configuration interaction (RASCI),<sup>79–81</sup> generalized active space self-consistent field (GASSCF),<sup>82–85</sup> and density matrix renormalization group (DMRG)<sup>86–88</sup> methods. In addition to that, the wave function framework can be completely abandoned in MC-PDFT by using the variational 2-RDM method, where the 2-RDM is computed directly under the constraint of  $N$ -representability conditions.<sup>89</sup> All these approximations aim to reduce the computational cost that scales exponentially with the system size so that the larger number of electrons can be correlated, which is important in strongly correlated systems. Here, we explored another appealing opportunity that is combining MC-PDFT calculations with 2-RDM simulations performed on the quantum computer. The 1-RDMs were contracted from the QACSE 2-RDMs, and the PDFT step was performed on the classical computer. To estimate the sensitivity of predicted ground state energies to the choice of the on-top functional, we explored several types of functionals including (i) translated<sup>28</sup> (tPBE and tBLYP), (ii) fully translated<sup>39</sup> (ftPBE), and (iii) hybrid<sup>40</sup> (tPBE0) on-top functionals. Note that translation of Kohn–Sham density functionals into the on-top density functionals does not alter the functional form but redefines the spin-densities and their gradients in terms of the total electron density and the on-top pair density.

#### REFERENCES

- W. Kohn and L. J. Sham, "Self-consistent equations including exchange and correlation effects," *Phys. Rev.* **140**, A1133–A1138 (1965).
- K. Head-Marsden, J. Flick, C. J. Ciccarino, and P. Narang, "Quantum information and algorithms for correlated quantum matter," *Chem. Rev.* **121**, 3061–3120 (2021).
- M. Reiher, N. Wiebe, K. M. Svore, D. Wecker, and M. Troyer, "Elucidating reaction mechanisms on quantum computers," *Proc. Natl. Acad. Sci. U. S. A.* **114**, 7555–7560 (2017).
- D. Zhang and D. G. Truhlar, *J. Chem. Theory Comput.* **17**, 5733–5744 (2021).
- C. L. Benavides-Riveros, N. N. Lathiotakis, and M. A. L. Marques, *Phys. Chem. Chem. Phys.* **19**, 12655–12664 (2017).
- D. Roca-Sanjuán, F. Aquilante, and R. Lindh, "Multiconfiguration second-order perturbation theory approach to strong electron correlation in chemistry and photochemistry," *Wiley Interdiscip. Rev.: Comput. Mol. Sci.* **2**, 585–603 (2012).
- B. M. Austin, D. Y. Zubarev, and W. A. Lester, "Quantum Monte Carlo and related approaches," *Chem. Rev.* **112**, 263–288 (2012).
- T. Yanai and G. K.-L. Chan, "Canonical transformation theory for multireference problems," *J. Chem. Phys.* **124**, 194106 (2006).
- T. Yanai, Y. Kurashige, E. Neuscamman, and G. K.-L. Chan, "Multireference quantum chemistry through a joint density matrix renormalization group and canonical transformation theory," *J. Chem. Phys.* **132**, 024105 (2010).
- U. S. Mahapatra, B. Datta, and D. Mukherjee, "A size-consistent state-specific multireference coupled cluster theory: Formal developments and molecular applications," *J. Chem. Phys.* **110**, 6171–6188 (1999).
- C. Angeli, M. Pastore, and R. Cimiraglia, "New perspectives in multireference perturbation theory: The  $n$ -electron valence state approach," *Theor. Chem. Acc.* **117**, 743–754 (2007).
- V. E. Elfving, B. W. Broer, M. Webber, J. Gavartin, M. D. Halls, K. P. Lortton, and A. Bochevarov, "How will quantum computers provide an industrially relevant computational advantage in quantum chemistry?," [arXiv:2009.12472](https://arxiv.org/abs/2009.12472) (2020).
- S. McArdle, S. Endo, A. Aspuru-Guzik, S. C. Benjamin, and X. Yuan, "Quantum computational chemistry," *Rev. Mod. Phys.* **92**, 015003 (2020).

- <sup>14</sup>B. Bauer, S. Bravyi, M. Motta, and G. K.-L. Chan, "Quantum algorithms for quantum chemistry and quantum materials science," *Chem. Rev.* **120**, 12685–12717 (2020).
- <sup>15</sup>B. Bauer, D. Wecker, A. J. Millis, M. B. Hastings, and M. Troyer, "Hybrid quantum-classical approach to correlated materials," *Phys. Rev. X* **6**, 031045 (2016).
- <sup>16</sup>D. Dhawan, M. Metcalf, and D. Zgid, "Dynamical self-energy mapping (DSEM) for creation of sparse Hamiltonians suitable for quantum computing," *J. Chem. Theory Comput.* (published online 2021).
- <sup>17</sup>T. Keen, T. Maier, S. Johnston, and P. Lougovski, *Quantum Sci. Technol.* **5**, 035001 (2020).
- <sup>18</sup>N. C. Rubin, "A hybrid classical/quantum approach for large-scale studies of quantum systems with density matrix embedding theory," [arXiv:1610.06910](https://arxiv.org/abs/1610.06910) (2016).
- <sup>19</sup>T. Yamazaki, S. Matsuura, A. Narimani, A. Saidmuradov, and A. Zaribafyan, "Towards the practical application of near-term quantum computers in quantum chemistry simulations: A problem decomposition approach," [arXiv:1806.01305](https://arxiv.org/abs/1806.01305) (2018).
- <sup>20</sup>M. Metcalf, N. P. Bauman, K. Kowalski, and W. A. de Jong, "Resource-efficient chemistry on quantum computers with the variational quantum eigensolver and the double unitary coupled-cluster approach," *J. Chem. Theory Comput.* **16**, 6165–6175 (2020).
- <sup>21</sup>K. Kowalski and N. P. Bauman, "Sub-system quantum dynamics using coupled cluster downfolding techniques," *J. Chem. Phys.* **152**, 244127 (2020).
- <sup>22</sup>N. P. Bauman and K. Kowalski, [arXiv:2111.03215](https://arxiv.org/abs/2111.03215) (2021).
- <sup>23</sup>M. Motta, T. P. Gujarati, J. E. Rice, A. Kumar, C. Masteran, J. A. Latone, E. Lee, E. F. Valeev, and T. Y. Takeshita, "Quantum simulation of electronic structure with a transcorrelated Hamiltonian: Improved accuracy with a smaller footprint on the quantum computer," *Phys. Chem. Chem. Phys.* **22**, 24270–24281 (2020).
- <sup>24</sup>M. Urbanek, D. Camps, R. Van Beeumen, and W. A. de Jong, "Chemistry on quantum computers with virtual quantum subspace expansion," *J. Chem. Theory Comput.* **16**, 5425–5431 (2020).
- <sup>25</sup>T. Takeshita, N. C. Rubin, Z. Jiang, E. Lee, R. Babbush, and J. R. McClean, "Increasing the representation accuracy of quantum simulations of chemistry without extra quantum resources," *Phys. Rev. X* **10**, 011004 (2020).
- <sup>26</sup>S. E. Smart and D. A. Mazziotti, "Quantum solver of contracted eigenvalue equations for scalable molecular simulations on quantum computing devices," *Phys. Rev. Lett.* **126**, 070504 (2021).
- <sup>27</sup>D. A. Mazziotti, "Anti-Hermitian contracted Schrödinger equation: Direct determination of the two-electron reduced density matrices of many-electron molecules," *Phys. Rev. Lett.* **97**, 143002 (2006).
- <sup>28</sup>G. Li Manni, R. K. Carlson, S. Luo, D. Ma, J. Olsen, D. G. Truhlar, and L. Gagliardi, "Multiconfiguration pair-density functional theory," *J. Chem. Theory Comput.* **10**, 3669–3680 (2014).
- <sup>29</sup>S. E. Smart, J.-N. Boyn, and D. A. Mazziotti, "Resolving correlated states of benzene on a quantum computer with an error-mitigated quantum contracted eigenvalue solver," [arXiv:2103.06876](https://arxiv.org/abs/2103.06876) (2021).
- <sup>30</sup>D. A. Mazziotti, "Realization of quantum chemistry without wave functions through first-order semidefinite programming," *Phys. Rev. Lett.* **93**, 213001 (2004).
- <sup>31</sup>D. A. Mazziotti, "Structure of fermionic density matrices: Complete  $n$ -representability conditions," *Phys. Rev. Lett.* **108**, 263002 (2012).
- <sup>32</sup>J. Foley and D. A. Mazziotti, *Phys. Rev. A* **86**, 012512 (2012).
- <sup>33</sup>N. C. Rubin, R. Babbush, and J. McClean, *New J. Phys.* **20**, 053020 (2018).
- <sup>34</sup>A. M. Sand and D. A. Mazziotti, "Enhanced computational efficiency in the direct determination of the two-electron reduced density matrix from the anti-Hermitian contracted Schrödinger equation with application to ground and excited states of conjugated  $\pi$ -systems," *J. Chem. Phys.* **143**, 134110 (2015).
- <sup>35</sup>J.-N. Boyn and D. A. Mazziotti, "Accurate singlet-triplet gaps in biradicals via the spin averaged anti-Hermitian contracted Schrödinger equation," *J. Chem. Phys.* **154**, 134103 (2021).
- <sup>36</sup>A. E. DePrince and D. A. Mazziotti, "Cumulant reconstruction of the three-electron reduced density matrix in the anti-Hermitian contracted Schrödinger equation," *J. Chem. Phys.* **127**, 104104 (2007).
- <sup>37</sup>D. A. Mazziotti, "Comparison of contracted Schrödinger and coupled-cluster theories," *Phys. Rev. A* **60**, 4396–4408 (1999).
- <sup>38</sup>D. A. Mazziotti, "Approximate solution for electron correlation through the use of Schwinger probes," *Chem. Phys. Lett.* **289**, 419–427 (1998).
- <sup>39</sup>R. K. Carlson, D. G. Truhlar, and L. Gagliardi, "Multiconfiguration pair-density functional theory: A fully translated gradient approximation and its performance for transition metal dimers and the spectroscopy of  $\text{Re}_2\text{Cl}_8^{2-}$ ," *J. Chem. Theory Comput.* **11**, 4077–4085 (2015).
- <sup>40</sup>R. Pandharkar, M. R. Hermes, D. G. Truhlar, and L. Gagliardi, "A new mixing of nonlocal exchange and nonlocal correlation with multiconfiguration pair-density functional theory," *J. Phys. Chem. Lett.* **11**, 10158–10163 (2020).
- <sup>41</sup>Maplesoft, a division of Waterloo Maple, Inc., Waterloo, Ontario, Maple, 2021.
- <sup>42</sup>RDMChem, Chicago, Illinois, Quantum chemistry toolbox, 2021.
- <sup>43</sup>Q. Sun, T. C. Berkelbach, N. S. Blunt, G. H. Booth, S. Guo, Z. Li, J. Liu, J. D. McClain, E. R. Sayfutyarova, S. Sharma, S. Wouters, and G. K.-L. Chan, "PySCF: The Python-based simulations of chemistry framework," *Wiley Interdiscip. Rev.: Comput. Mol. Sci.* **8**, e1340 (2018).
- <sup>44</sup>M. R. Hermes, "mrh," GitHub. <https://github.com/MatthewRHermes/mrh>.
- <sup>45</sup>W. Sander, "*m*-benzyne and *p*-benzyne," *Acc. Chem. Res.* **32**, 669–676 (1999).
- <sup>46</sup>A. V. Dubrovskiy, N. A. Markina, and R. C. Larock, "Use of benzenes for the synthesis of heterocycles," *Org. Biomol. Chem.* **11**, 191–218 (2013).
- <sup>47</sup>P. G. Wentholt, R. R. Squires, and W. C. Lineberger, "Ultraviolet photoelectron spectroscopy of the *o*-, *m*-, and *p*-benzyne negative ions. Electron affinities and singlet-triplet splittings for *o*-, *m*-, and *p*-benzyne," *J. Am. Chem. Soc.* **120**, 5279–5290 (1998).
- <sup>48</sup>T. H. Dunning, "Gaussian basis sets for use in correlated molecular calculations. I. The atoms boron through neon and hydrogen," *J. Chem. Phys.* **90**, 1007–1023 (1989).
- <sup>49</sup>D. A. Mazziotti, "Extraction of electronic excited states from the ground-state two-particle reduced density matrix," *Phys. Rev. A* **68**, 052501 (2003).
- <sup>50</sup>L. Greenman and D. A. Mazziotti, "Electronic excited-state energies from a linear response theory based on the ground-state two-electron reduced density matrix," *J. Chem. Phys.* **128**, 114109 (2008).
- <sup>51</sup>S. Hemmatiyan, M. Sajjan, A. W. Schlimgen, and D. A. Mazziotti, "Excited-state spectra of strongly correlated molecules from a reduced-density-matrix approach," *J. Phys. Chem. Lett.* **9**, 5373–5378 (2018).
- <sup>52</sup>V. von Burg, G. H. Low, T. Häner, D. S. Steiger, M. Reiher, M. Roetteler, and M. Troyer, "Quantum computing enhanced computational catalysis," *Phys. Rev. Res.* **3**, 033055 (2021).
- <sup>53</sup>D. A. Mazziotti, "Contracted Schrödinger equation: Determining quantum energies and two-particle density matrices without wave functions," *Phys. Rev. A* **57**, 4219–4234 (1998).
- <sup>54</sup>D. A. Mazziotti, "Anti-Hermitian formulation of the contracted Schrödinger theory," in *Reduced-Density-Matrix Mechanics: With Application to Many-Electron Atoms and Molecules*, Advances in Chemical Physics Vol. 134, edited by D. A. Mazziotti (Wiley, New York, 2007), p. 331.
- <sup>55</sup>D. A. Mazziotti, "Anti-Hermitian part of the contracted Schrödinger equation for the direct calculation of two-electron reduced density matrices," *Phys. Rev. A* **75**, 022505 (2007).
- <sup>56</sup>D. A. Mazziotti, "3,5-contracted Schrödinger equation: Determining quantum energies and reduced density matrices without wave functions," *Int. J. Quantum Chem.* **70**, 557–570 (1998).
- <sup>57</sup>F. Colmenero, C. Pérez del Valle, and C. Valdemoro, "Approximating  $q$ -order reduced density matrices in terms of the lower-order ones. I. General relations," *Phys. Rev. A* **47**, 971–978 (1993).
- <sup>58</sup>D. A. Mazziotti, "Two-electron reduced density matrices from the anti-Hermitian contracted Schrödinger equation: Enhanced energies and properties with larger basis sets," *J. Chem. Phys.* **126**, 184101 (2007).
- <sup>59</sup>D. A. Mazziotti, "Multireference many-electron correlation energies from two-electron reduced density matrices computed by solving the anti-Hermitian contracted Schrödinger equation," *Phys. Rev. A* **76**, 052502 (2007).
- <sup>60</sup>J. W. Snyder and D. A. Mazziotti, "Conical intersection of the ground and first excited states of water: Energies and reduced density matrices from the anti-Hermitian contracted Schrödinger equation," *J. Phys. Chem. A* **115**, 14120–14126 (2011).

- <sup>61</sup>J. W. Snyder and D. A. Mazziotti, "Photoexcited conversion of gauche-1,3-butadiene to bicyclobutane via a conical intersection: Energies and reduced density matrices from the anti-Hermitian contracted Schrödinger equation," *J. Chem. Phys.* **135**, 024107 (2011).
- <sup>62</sup>S. E. Smart, P. G. Scrape, L. J. Butler, and D. A. Mazziotti, "Using reduced density matrix techniques to capture static and dynamic correlation in the energy landscape for the decomposition of the CH<sub>2</sub>CH<sub>2</sub>ONO radical and support a non-IRC pathway," *J. Chem. Phys.* **149**, 024302 (2018).
- <sup>63</sup>G. Gidofalvi and D. A. Mazziotti, "Direct calculation of excited-state electronic energies and two-electron reduced density matrices from the anti-Hermitian contracted Schrödinger equation," *Phys. Rev. A* **80**, 022507 (2009).
- <sup>64</sup>E. J. Sturm and D. A. Mazziotti, "Highly accurate excited-state energies from direct computation of the 2-electron reduced density matrix by the anti-Hermitian contracted Schrödinger equation," *Mol. Phys.* **114**, 335–343 (2016).
- <sup>65</sup>X. Bonet-Monroig, R. Babbush, and T. E. O'Brien, "Nearly optimal measurement scheduling for partial tomography of quantum states," *Phys. Rev. X* **10**, 031064 (2020).
- <sup>66</sup>S. E. Smart and D. A. Mazziotti, "Lowering tomography costs in quantum simulation with a symmetry projected operator basis," *Phys. Rev. A* **103**, 012420 (2021).
- <sup>67</sup>IBM quantum, 2020.
- <sup>68</sup>H. Abraham, AduOffei, R. Agarwal, I. Y. Akhalwaya, G. Aleksandrowicz, T. Alexander, M. Amy, E. Arbel, Arjjit02, A. Asfaw, A. Avkhadiev, C. Azaustre, AzizNgoueya, A. Banerjee, A. Bansal, P. Barkoutsos, G. Barron, G. S. Barron, L. Bello, Y. Ben-Haim, D. Bevenius, A. Bhobe, L. S. Bishop *et al.* (2021), "Qiskit: An open-source framework for quantum computing," Zenodo. <https://doi.org/10.5281/zenodo.2573505>.
- <sup>69</sup>K. Setia, R. Chen, J. E. Rice, A. Mezzacapo, M. Pistoia, and J. D. Whitfield, "Reducing qubit requirements for quantum simulations using molecular point group symmetries," *J. Chem. Theory Comput.* **16**, 6091–6097 (2020).
- <sup>70</sup>S. E. Smart and D. A. Mazziotti, "HQCA: Hybrid quantum computing algorithms for quantum chemistry," GitHub. <https://github.com/damazz/HQCA>.
- <sup>71</sup>P. G. Szalay, T. Müller, G. Gidofalvi, H. Lischka, and R. Shepard, "Multiconfiguration self-consistent field and multireference configuration interaction methods and applications," *Chem. Rev.* **112**, 108–181 (2012).
- <sup>72</sup>J. P. Perdew, A. Savin, and K. Burke, "Escaping the symmetry dilemma through a pair-density interpretation of spin-density functional theory," *Phys. Rev. A* **51**, 4531–4541 (1995).
- <sup>73</sup>A. O. Lykhin, D. G. Truhlar, and L. Gagliardi, "Role of triplet states in the photodynamics of aniline," *J. Am. Chem. Soc.* **143**, 5878–5889 (2021).
- <sup>74</sup>A. M. Sand, K. M. Kidder, D. G. Truhlar, and L. Gagliardi, "Calculation of chemical reaction barrier heights by multiconfiguration pair-density functional theory with correlated participating orbitals," *J. Phys. Chem. A* **123**, 9809–9817 (2019).
- <sup>75</sup>S. S. Dong, L. Gagliardi, and D. G. Truhlar, "Excitation spectra of retinal by multiconfiguration pair-density functional theory," *Phys. Chem. Chem. Phys.* **20**, 7265–7276 (2018).
- <sup>76</sup>A. M. Sand, D. G. Truhlar, and L. Gagliardi, "Efficient algorithm for multiconfiguration pair-density functional theory with application to the heterolytic dissociation energy of ferrocene," *J. Chem. Phys.* **146**, 034101 (2017).
- <sup>77</sup>P. Sharma, V. Bernales, D. G. Truhlar, and L. Gagliardi, "Valence  $\pi\pi^*$  excitations in benzene studied by multiconfiguration pair-density functional theory," *J. Phys. Chem. Lett.* **10**, 75–81 (2019).
- <sup>78</sup>P. Sharma, D. G. Truhlar, and L. Gagliardi, "Multiconfiguration pair-density functional theory investigation of the electronic spectrum of MnO<sup>4-</sup>," *J. Chem. Phys.* **148**, 124305 (2018).
- <sup>79</sup>D. Presti, D. G. Truhlar, and L. Gagliardi, "Intramolecular charge transfer and local excitation in organic fluorescent photoredox catalysts explained by RASCI-PDFT," *J. Phys. Chem. C* **122**, 12061–12070 (2018).
- <sup>80</sup>A. M. Sand, C. E. Hoyer, D. G. Truhlar, and L. Gagliardi, "State-interaction pair-density functional theory," *J. Chem. Phys.* **149**, 024106 (2018).
- <sup>81</sup>D. Presti, S. J. Stoneburner, D. G. Truhlar, and L. Gagliardi, "Full correlation in a multiconfigurational study of bimetallic clusters: Restricted active space pair-density functional theory study of [2Fe–2S] systems," *J. Phys. Chem. C* **123**, 11899–11907 (2019).
- <sup>82</sup>S. O. Odoh, G. L. Manni, R. K. Carlson, D. G. Truhlar, and L. Gagliardi, "Separated-pair approximation and separated-pair pair-density functional theory," *Chem. Sci.* **7**, 2399–2413 (2016).
- <sup>83</sup>S. Ghosh, C. J. Cramer, D. G. Truhlar, and L. Gagliardi, "Generalized-active-space pair-density functional theory: An efficient method to study large, strongly correlated, conjugated systems," *Chem. Sci.* **8**, 2741–2750 (2017).
- <sup>84</sup>J. L. Bao, S. O. Odoh, L. Gagliardi, and D. G. Truhlar, "Predicting bond dissociation energies of transition-metal compounds by multiconfiguration pair-density functional theory and second-order perturbation theory based on correlated participating orbitals and separated pairs," *J. Chem. Theory Comput.* **13**, 616–626 (2017).
- <sup>85</sup>S. J. Li, L. Gagliardi, and D. G. Truhlar, "Extended separated-pair approximation for transition metal potential energy curves," *J. Chem. Phys.* **152**, 124118 (2020).
- <sup>86</sup>P. Sharma, D. G. Truhlar, and L. Gagliardi, "Magnetic coupling in a tris-hydroxo-bridged chromium dimer occurs through ligand mediated superexchange in conjunction with through-space coupling," *J. Am. Chem. Soc.* **142**, 16644–16650 (2020).
- <sup>87</sup>P. Sharma, V. Bernales, S. Knecht, D. G. Truhlar, and L. Gagliardi, "Density matrix renormalization group pair-density functional theory (DMRG-PDFT): Singlet–triplet gaps in polyacenes and polyacetylenes," *Chem. Sci.* **10**, 1716–1723 (2019).
- <sup>88</sup>C. Zhou, L. Gagliardi, and D. G. Truhlar, "Multiconfiguration pair-density functional theory for iron porphyrin with CAS, RAS, and DMRG active spaces," *J. Phys. Chem. A* **123**, 3389–3394 (2019).
- <sup>89</sup>M. Mostafanejad and A. E. DePrince, "Combining pair-density functional theory and variational two-electron reduced-density matrix methods," *J. Chem. Theory Comput.* **15**, 290–302 (2019).